Biochimie 200 (2022) 79–86

Contents lists available at ScienceDirect

Biochimie

journal homepage: www.elsevier.com/locate/biochi

Tau R2 and R3 are essential regions for tau aggregation, seeding and propagation

Narendran Annadurai [a], Lukáš Malina [b], Jakub Malohlava [b], Marián Hajdúch [a, c], Viswanath Das [a, c, *]

[a] Institute of Molecular and Translational Medicine, Faculty of Medicine and Dentistry, Palacký University Olomouc, Hněvotínská 1333/5, 77900, Olomouc, Czech Republic
[b] Department of Medical Biophysics, Faculty of Medicine and Dentistry, Palacký University in Olomouc, Olomouc, Czech Republic
[c] Czech Advanced Technologies and Research Institute (CATRIN), Institute of Molecular and Translational Medicine, Palacký University Olomouc, Krizkovskeho 511/8, 77900, Olomouc, Czech Republic

ARTICLE INFO

Article history:
Received 6 August 2021
Received in revised form
20 May 2022
Accepted 20 May 2022
Available online 24 May 2022

Keywords:
Alzheimer's disease
Tau aggregation
Tau phosphorylation
Prion-like
Tau seeding
Propagation

ABSTRACT

Tauopathies are characterised by intracellular deposits of fibrillar tau tangles. However, the interneuronal spread of pathological tau species precedes the development of major tau burdens. Two amyloid motifs, VQIINK in repeat 2 and VQIVYK in repeat 3, of tau repeat domain, assemble into β-sheet-rich fibrils on their own but alone do not form seed-competent fibrils. In contrast, the entire R3 region self-aggregates and forms seed-competent fibrils. Our study aimed to identify the minimal regions in the tau repeat domain that define seeding and its impact on intracellular tau phosphorylation and aggregation. Using peptides of individual repeats, we show that R2, like R3, forms seed-competent fibrils when assembled in the presence of heparin. However, R3, but not R2, forms seed-competent fibrils when assembled without heparin, even though both R2 and R3 have identical N-terminal hexapeptide and cysteine residue sequences. Moreover, cysteine to alanine substitution in R3 abrogates its self-aggregation and seeding potency. Tau RD P301S biosensor cells and Tau P301L (0N4R)-expressing HEK293 cells seeded with R2 and R3 fibrils show the induction of pathological phosphorylation of tau at Ser262/Ser396/Ser404 positions and oligomerisation of native tau. Protein fractions of biosensor cells seeded with R2 and R3 fibrils reseed endogenous tau aggregation when introduced into a fresh set of biosensor cells. Our findings suggest that R3 may be the minimal region for pathological seed generation under physiological conditions, whereas R2 might need polyanionic cofactors to generate pathogenic seeds. Lastly, R2 and R3 fibrils induce template-induced misfolding and pathological hyperphosphorylation of intracellular tau, making intracellular tau seed-competent.

1. Introduction

Tauopathies, such as Alzheimer's disease (AD), are defined by intracellular deposits of microtubule-associated tau protein and transcellular propagation of tau seeds. Hyperphosphorylation is one of the critical disease-associated posttranslational modifications (PTMs) of tau in AD that affects its structure, distribution, and functions [1]. However, some specific phosphoepitopes are exclusively present in AD brains [2]. Evidence supports the role of soluble and highly phosphorylated toxic prion-like tau strains in mediating synaptic dysfunctions and neuronal loss [3–5]. When injected into the hippocampus of transgenic mice expressing human tau, AD brain samples generate reducing agent-resistant hyperphosphorylated fibrils of seeded tau [6]. The formed fibrils are also resistant to dephosphorylation by protein phosphatase 2A [6]. Dephosphorylation of AD-derived hyperphosphorylated tau strongly reduces seeding following intracerebral injection in hTau mice that express all six isoforms of nonmutated human tau encoded by the genomic human tau transgene [7]. However, this could be due to the less susceptibility of wild-type tau to hyperphosphorylation than mutant tau.

* Corresponding author. Institute of Molecular and Translational Medicine, Faculty of Medicine and Dentistry, Palacký University Olomouc, Hněvotínská 1333/5, 77900, Olomouc, Czech Republic.
E-mail address: viswanath.das@upol.cz (V. Das).

https://doi.org/10.1016/j.biochi.2022.05.013
0300-9084/

Several cell models and *in vivo* studies show that tau fibrils from mutant P301S tau-expressing mice or tauopathy patients result in detergent-insoluble hyperphosphorylated fibrils of seeded tau [8–10]. Furthermore, the detergent-insoluble native human P301S tau fibrils in transgenic mice are more potent in seeding than fibrils of unphosphorylated or hyperphosphorylated recombinant tau [11]. Overall, evidence proves that pathological hyperphosphorylations induce changes that affect tau seeds and the seeded tau, contributing to tau propagation and its consequences in AD.

Tau forms self-replicating seeds that create unique pathological patterns in cells and animal models [12–15]. These uniquely structured seeds escape from affected cells and act as functional templates to trigger native tau aggregation when internalised by neighbouring cells [16]. Transcellular propagation of tau fibrils is a common feature of several tauopathies, including AD, where synaptic tau seeding precedes the spread of tau pathology [16–18]. The microtubule-binding domain of tau is essential for its aggregation [19,20] and phosphorylation at Ser202/Thr205/Ser208 sites in the proline-rich domain drives rapid fibrillisation [21]. Data indicate that two amyloid motifs, VQIINK in repeat 2 (R2) and VQIVYK in repeat 3 (R3), in tau repeat domain (RD) assemble *in vitro* into β-sheet-rich fibrils, but these fibrils are not seed-competent [22]. However, 31-amino acid peptides of the R3 region self-assemble into seed-competent fibrils [23,24]. Deleting VQIINK or VQIVYK in recombinant full-length tau impairs the seeding ability, suggesting that the amyloid motifs are necessary for seeding [11].

We used peptides of individual tau repeats to study each repeat's aggregation and seeding potency using cell lines expressing aggregation-prone P301S and P301L tau (Fig. 1A). Cells seeded with extracellular R2 and R3 fibrils induce intracellular tau aggregation, and the formed intracellular tau fibrils are majorly triton-insoluble and phosphorylated at AD-specific sites. Furthermore, reseeding cells with intracellular fibrils extracted from R2 and R3 fibrils-seeded biosensor cells continue to propagate tau aggregation. Our findings suggest that β-sheet-rich R2 and R3 fibrils induce templated misfolding and pathological hyperphosphorylation of seeded tau into seed-competent intracellular inclusions.

2. Materials and methods

2.1. Cell culture and DNA transfection

Tau RD P301S FRET biosensor cells (Biosensor cells; ATCC® CRL-3275™) were cultured in Dulbecco's Modified Eagle's medium (Lonza, Cat. # 12–604F) supplemented with 1% GlutaMAX (Gibco, Cat. #35050-061), 10% fetal calf serum (Gibco, Cat. # 10270) and 1% penicillin/streptomycin (Diagnovum, Cat. # 910). Human embryonic kidney HEK293 cells (ATCC® CRL-1573™) were cultured in Eagle's Minimum Essential Medium (Lonza, Cat. # 12–611F) supplemented with 10% fetal calf serum and 1% penicillin/streptomycin. The cell lines were maintained at 37 °C in a 5%-CO_2 incubator and routinely tested for mycoplasma contamination.

Tau P301L (0N4R) plasmid cloned in pCMV6 was a kind gift from Dr Jose F Abisambra of the University of Kentucky (Lexington, KY, USA). HEK293 cells were plated at a density of 1 x 10^6/mL plated in

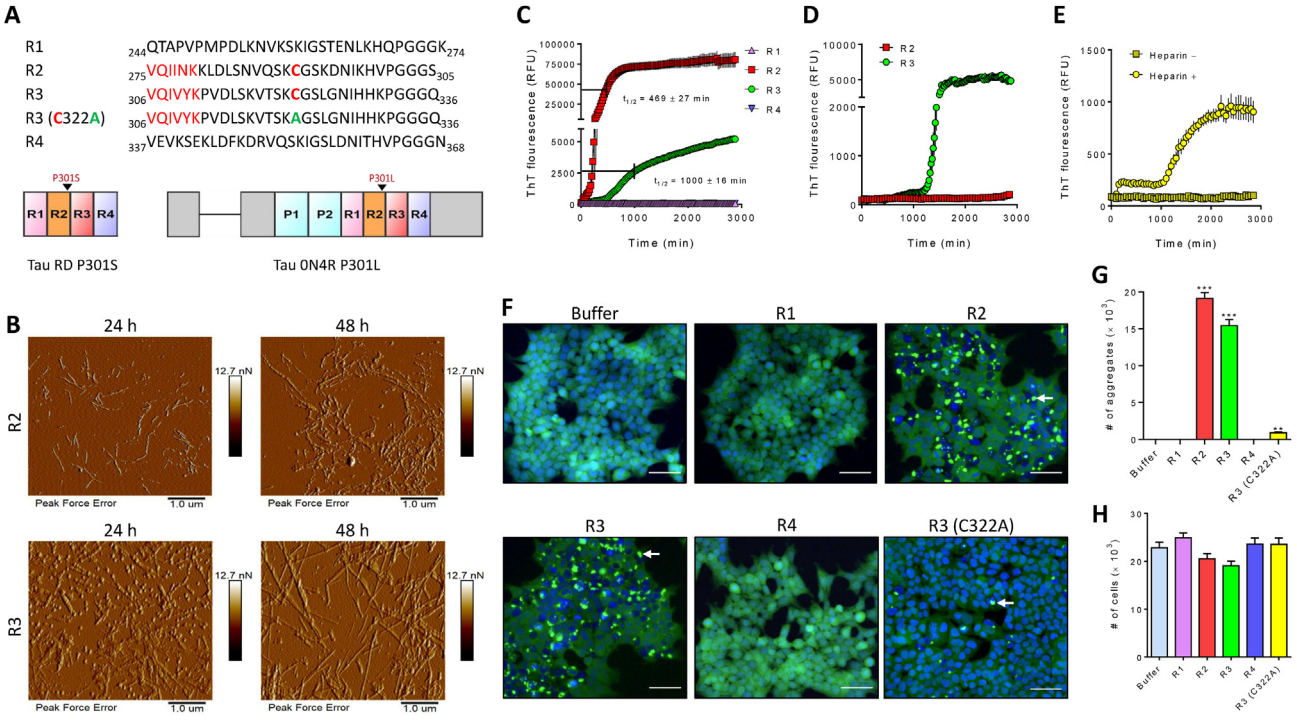

Fig. 1. Aggregation of tau repeat peptides and seeding. (A) Amino acid sequences of different tau peptides used in the study and schematic representation of tau constructs in Tau RD P301S FRET biosensor cells and HEK293 Tau 0N4R P301L cells are shown. The sequence numbering in the peptides is according to the 2N4R tau isoform (441 amino acid residues). The N-terminal hexapeptide regions are marked in red, the cysteine residues are marked in bold red, and the cysteine to alanine substitution at position 322 in the R3 (C322A) peptide is shown in green in the amino acid sequences. (B) AFM images of R2 and R3 fibrils formed after 24 and 48 h of aggregation. (C–E) Aggregation of peptides at 25 μM concentration in the presence of heparin (C), 25 μM R2 and R3 peptides in the absence of heparin (D), and 10 μM R3 (C322A) peptide in the absence or presence of heparin (E). Data in C-E are mean ± SEM of 3 independent replicates. (F) Seeding of Tau RD P301S in biosensor cells after 72 h of treatment with buffer (containing heparin) or 50 nM R1, R2, R3, R4 and R3 (C322A) samples or fibrils assembled in the presence of heparin. Scale bar: 50 μm. (G–H) The number of seeded intracellular Tau RD P301S aggregates (G) and cells after treatment as indicated in (H). Data are mean ± SEM of 3 independent experiments. ***p < 0.001, **p < 0.01 *vs* buffer-treated cells, one-way ANOVA, Dunnett's posthoc test.

a 100 mm tissue culture Petri dish and transfected with 2 μg/mL Tau P301L plasmid diluted in jetPRIME® buffer supplemented with jetPRIME® reagent following the manufacturer's protocol for 18 h.

2.2. Tau aggregation assay

Tau R1 (Cat. # AS-65433-1), R2 (AS-65434-1), R3 (AS-65435-1), and R4 (AS-65436-1) peptides were purchased from AnaSpec (Fremont, CA, USA), and mutant R3 (C322A) peptides were purchased from Genscript Biotech (Piscataway, NJ, USA) dissolved in sterilised deionised water, and stored at −80 °C until further use. Peptide aggregation was monitored by an *in vitro* Thioflavin T (ThT) binding assay. Briefly, the peptide solution stored at −80 °C was thawed on ice and centrifuged at 13000 rpm for 45 s on a benchtop centrifuge. A reaction mixture containing 0–50 μM peptides and 15 μM ThT (Sigma-Aldrich, Cat. #T3516-5G) was prepared in peptide aggregation buffer [20 mM Tris (pH 7.4), 100 mM NaCl, 1 mM EDTA] with or without 5 μM heparin (Sigma-Aldrich, Cat. #H4784-1G) in an ice-chilled 1.5 mL Eppendorf tube. The reaction mixture was then dispensed into a black, clear-bottom 384-well assay plate (CellCarrier, Cat. # 6007550; PerkinElmer, Waltham, MA, USA), followed by sealing the plate with a TopSealA-PLUS (PerkinElmer) Clear Adhesive Seal to prevent evaporation. Throughout sample preparation, reagents and the assay plate were kept on ice. Following the addition of reagents, the assay plate was placed in an EnSpire Multimode Plate Reader (PerkinElmer), with the temperature of the measurement chamber set to 37 °C. To prevent condensation in the sealed plate, the upper heater temperature was set to 2 °C warmer than the lower heater temperature. The plate reader was set to maintain the assay plate under constant agitation (1000 rpm) during the resting period. The fluorescence of ThT binding to aggregated peptides was recorded every 5 min up to 48 h (λexc = 460–490 nm, λem = 500–550 nm).

For the 8-anilino-1-naphthalenesulfonic acid (ANS) fluorescence assay, 25 μM peptides were aggregated in peptide aggregation buffer containing 40 μM ANS (Sigma-Aldrich, Cat. #A1028-5G) with or without 5 μM heparin under similar aggregation conditions as described in ThT assay. The change in ANS fluorescence (λexc 390 nm/λem 475 nm) was recorded using EnSpire Multimode Plate Reader (PerkinElmer).

2.3. Fluorescence and atomic force microscopy

To visualise the formation of peptide fibrils, the content of wells from assay plates following the end of the ThT binding assay was embedded in 0.05% low-melting agarose (Sigma-Aldrich) cooled to 40 °C for 10–15 min at room temperature. The images of ThT-stained fibrils were captured on an Operetta™ High-Content Imaging System (PerkinElmer) using a 2 × objective (numerical aperture: 0.08) and 488-laser line (λex/λem: 488 nm/509 nm).

The morphology of fibrils formed 24 and 48 h after aggregation was confirmed by atomic force microscopy (AFM). Collected samples were added dropwise onto a freshly cleaved 10 mm-sized AFM mica disc (Ted Pella, Inc., Redding, CA) and air-dried for 10 min at room temperature. The mica discs were washed 5 × times with a 0.22 μm sterile syringe filter (Merck Millipore, Burlington, MA)-sterilised deionised water and dried for 10–15 min at room temperature. The discs were strapped on a glass slide using transparent cello tape to prevent them from moving during imaging. Images were acquired on an Olympus IX81/Veeco BioScope™ Catalyst™ Atomic Force Microscope (Bruker, Billerica, CA, USA) using a 10 × objective under ambient conditions at a scan rate of 0.7 Hz (line/sec) and Peak Force amplitude of 150 nm. Antimony doped silicon cantilever probe with a typical resonant frequency of 150 Hz and spring constant of 5.1 Nm^{-1} were employed, and acquired images were processed in Gwyddion 2.40 freeware developed by the Czech Metrology Institute, Brno, Czech Republic.

2.4. Coomassie gel staining

R2 and R3 fibrils collected after 24 and 48 h of aggregation assay were centrifuged at 65 000×*g* on a benchtop centrifuge for 60 min at 4 °C to pellet insoluble fractions. The soluble fractions were removed, and the pellet fractions were washed twice with 1 × PBS by centrifugation at 65 000×*g* for 5 min. The pelleted samples were then electrophoresed and processed for Coomassie staining, as described elsewhere [25].

2.5. Tau seeding assay

Tau RD P301S biosensor cells and Tau P301L (0N4R) HEK293 cells were plated at a density of 50,000 cells/mL in a CellCarrier 96-well plate (PerkinElmer, Cat. # 6005550) for imaging experiments or at a density of 1 x 10^6 cells/mL for cellular fractionation in TPP Ø96mm, 60 cm^2 tissue culture Petri dishes (TPP Techno Plastic Products AG, Trasadingen, Switzerland). The next day, cells were transfected with 50 nM or 100 nM peptide fibrils, collected from the *in vitro* aggregation assay carried out in the absence of ThT, premixed in jetPRIME® Buffer (Polyplus-transfection SA, New York, NY, USA) supplemented with jetPRIME® reagent (Polyplus-transfection SA) as described elsewhere [25]. A mixture of transfection reagents without tau peptides in peptide aggregation buffer was used as a negative seeding control. Twenty-four hours after transfection, the old medium was replaced with a fresh complete growth medium. The cells were allowed to grow for 48 h before processing for imaging and Triton X-100 fractionation cell fractionation experiments.

2.6. Imaging and quantification of aggregate and cell number

Prior to imaging, the biosensor cells were stained with 10 μM Hoechst-33342 nuclear dye (Invitrogen, Cat. #H21492) for 10–15 min at 37 °C in a humidified incubator, and the cells were replaced with phenol red-free growth media and imaged on an Operetta™ High-Content Imaging System (PerkinElmer) using a 20x objective as described elsewhere [25]. The intracellular CFP/YFP Tau RD P301S fibrils and cell numbers were quantified using Harmony Image Analysis Software as described in our previous work [25]. For morphology, the cells were imaged on Cell Voyager CV7000S microscope (Yokogawa, Tokyo, Japan) using a 60x objective. Cells were maintained at 37 °C and 5% CO_2/atmospheric air throughout imaging in a live-cell chamber.

2.7. Quantification of internalised R3 fibrils

R3 fibrils were stained with 50 nM X-34 (Sigma-Aldrich, Cat. # SML1954) for 5 min at room temperature. HEK293 cells were then transfected with R3 fibrils prestained with X-34 premixed with or without transfection reagent as described above. After 12 h of transfection, cells were washed with 1 × PBS containing 20 U/mL heparin (Cat. #H4784-1G, Sigma-Aldrich) and then 0.25% trypsin (Gibco) in PBS for 2–3 min to remove any cell membrane-bound fibrils that were not internalised. Prior to imaging, the cells were stained with 1x BioTracker 650 Red Nuclear Dye (Merck Millipore, Cat. # SCT119), and the old medium was replaced with a phenol red-free medium. Cells were imaged on a ZEISS Cell Observer SD Spinning Disk Confocal Microscope (Carl Zeiss AG, Oberkochen, Germany) using an oil-immersion 63 × objective (numerical aperture: 1.4). Images were acquired using ZEN 2 (blue edition) software (Carl Zeiss AG). X-34 was excited with a 405-nm laser line

(λexc 350 nm/λem 470 nm), and BioTracker 650 Red Nuclear Dye was excited using a 639-nm laser line (λexc 650 nm/λem 665 nm). The laser intensity and exposure time were kept constant between different samples. The acquired images were processed using ZEN 2012 Black Edition imaging software (Carl Zeiss).

2.8. Triton X-100 cell fractionation and Western blot analysis

Cells were harvested and resuspended in 1 × Tris-Buffered Saline (TBS) containing 0.05% Triton X-100 supplemented with protease (Roche, Cat. # 04693116001) and phosphatase inhibitors (Roche, Cat. # 04906837001). The cell lysate was then clarified by centrifuging at 500×*g* for 5 min and 1000×*g* for another 5 min at 4 °C on a benchtop centrifuge. The supernatant was collected, and 20% of the supernatant fraction was stored as a total fraction. The remaining supernatant was centrifuged at 65,000×*g* for 30 min at 4 °C to collect the supernatant as Triton X-100-soluble fraction and pellet as Triton X-100-insoluble fraction. Finally, the pellet fraction was resuspended in RIPA buffer supplemented with protease and phosphatase inhibitors. Thirty-five μg of total fraction and the equal volume of Triton-soluble and -insoluble fractions were electrophoresed by 4–12% gradient PAGE and 10% SDS-PAGE.

Electrophoresed proteins were transferred onto a PVDF membrane (Blot™ 2 Transfer Stacks, PVDF, regular size, Invitrogen, Cat. # IB24001) using an iBlot™ 2 Gel Transfer Device (Thermofisher Scientific). The blots were blocked in 5% BSA in 1 × TBS containing 0.1% Tween® 20 Detergent (TBST) for 1 h at room temperature and incubated with primary antibodies, anti-tau A10 antibody (1:1000; SCBT, Cat. #sc-390476) and anti-tau Tau-5 antibody (1:1000; Invitrogen, Cat. #AHB0042), anti-phospho Ser202/Thr205 tau (1:1000; Invitrogen, Cat. #MN1020), anti-phospho Ser262 tau (1:1000; Invitrogen, Cat. #OPA1-03142), anti-phospho Ser396 tau (1:1000; Invitrogen, Cat. #44-752G), anti-phospho Ser404 tau (1:1000; CST, Cat. #20194S) and anti-oligomeric tau T22 (1:1000; Merck Millipore, Cat. #ABN454), overnight at 4 °C and anti-GAPDH antibody (1:4000; SCBT, Cat. #sc-32233) for 1 h at room temperature. Primary antibody-stained blots were developed using anti-mouse (Cat. #A1134) or anti-rabbit (Cat. #A21202) Alexa Fluor 488-conjugated secondary antibodies (Invitrogen) at 1:2000 dilution for 1–2 h at room temperature in the dark. The blots were then imaged using a Gel Doc XR + Gel Documentation System (Bio-Rad) with appropriate filters for Alexa Fluor 488 to visualise protein bands.

2.9. Cellular reseeding assay

Biosensor cells were plated at a density of 100,000 cells/ml in a CellCarrier 96-well plate (PerkinElmer). The next day, cells were transfected with 1 μg/well total and Triton-soluble and -insoluble fractions prepared from biosensor cells, as described previously. After 24 h of transfection, cells were replaced with fresh complete growth media, incubated further for 48 h, and then imaged on an OperettaTM high-content imaging system described above to quantify the cell number and intracellular Tau RD aggregates.

2.10. Statistical analysis

All statistical analyses were performed using Graphpad Prism Software, and differences were considered significant at $P < 0.05$.

3. Results

3.1. Self-assembling R3 is the minimal region of tau RD essential for aggregation

R2 and R3 peptides assembled time-dependently into β-sheet-rich fibrils in the presence of heparin, as evident by changes in fibril morphology and ThT fluorescence (Fig. 1B and C). Both R2 and R3 showed concentration-dependent growth kinetics (Fig. S1A). The aggregation data also show that R2 aggregates faster than R3, as indicated by the differences in $t_{1/2}$ values (R2 vs R3, $p < 0.001$, paired *t*-test, $n = 3$; Fig. 1C). R1 and R4 did not assemble into fibrils under the tested aggregation conditions (Fig.1C; Figs. S1A and B). The formation of β-sheet-rich fibrils of R2 and R3 was also validated by fluorescence imaging (Fig. S1C). These findings support a prior work that indicates VQIINK in R2 is a more powerful driver of tau aggregation than VQIVYK in R3 [26]. Nonetheless, both R2 and R3 formed dimers when aggregated in the presence of heparin (Fig. S2A). Surprisingly, despite having the amyloid VQIINK motif and a cysteine residue, R2 did not self-assemble into fibrils in the absence of heparin (Fig. 1D, Fig. S2B). R3 formed fibrils of highly-aggregated morphology with twists when aggregated in the absence of heparin compared to a mixture of shorter and longer fibrils without a twist in the presence of heparin (Fig. 1B, Fig. S2B).

To find if the cysteine residue is necessary for the self-assembly of R3, we used a cysteine to alanine substituted R3 peptide (C322A) (Fig. 1A). R3 (C322A) aggregated and formed fibrils in the presence but not in the absence of heparin (Fig. 1E; Fig. S2C). The fibrils comprised of a mixture of shorter and longer fibrils, morphologically similar to those of R3 fibrils formed in the presence of heparin (Fig. 1B, Fig. S2C). R3 (C322A) also showed concentration-dependent growth kinetics (Fig. S2D). This data indicates that cysteine residue in R3 is essential for self-assembly, which is accordant with the findings from Zweckstetter lab showing KXGS motifs in tau repeats promote aggregation [27].

We confirmed ThT data by ANS assay, which assess changes in hydrophobicity during protein aggregation, and noted a similar time-dependent increase in ANS fluorescence when peptides were aggregated in the presence [R2, R3, and R3 (C322A)] or absence (R3) of heparin (Figs. S2E and F).

3.2. R2 and R3 fibrils induce tau RD P301S aggregation in biosensor cells

Next, we performed an in-cell seeding assay using biosensor cells to check the seeding potential of repeat peptides collected 48 h after *in vitro* assembly. R2 and R3 fibrils, but not R1 and R4 samples, collected 48 h after assembly, seeded the aggregation of Tau RD P301S in cells (Fig. 1F and G). The aggregation buffer (containing transfection reagents) with or without heparin did not affect seeding or cell number (Fig. 1F–H; Fig. S3C). We previously observed that seeding requires the accumulation of exogenous seeds within the cell [25]. However, we did not quantify the percentage of R3 fibrils internalised by cells. Our data now show that in the presence of transfection reagent, a significant fraction of R3 fibrils is taken up by the cells (Figs. S3A and B). There is slow cellular uptake of fibrils in the absence of transfection reagents (Fig. S3B), which is presumably not enough to trigger seeding, as noted in our previous study [25].

Self-assembled fibrils of R3 demonstrated considerable seeding activity, in contrast to R2 and R3 (C322A) formed without heparin, which did not seed Tau RD P301S aggregation (Figs. S3C and D). Interestingly, despite C→A substitution, R3 (C322A) aggregated in the presence of heparin showed seeding activity (Fig. 1F and G). Nonetheless, R3 and R2 assembled with heparin were consistently

more seed-competent than fibrils of R3 assembled in the absence of heparin or R3 (C322A) in the presence of heparin. Overall, R2, R3 and R3 (C322A) fibrils assembled in the presence of heparin and R3 fibrils assembled in the absence of heparin resulted in intracellular tau seeding. This data highlights the importance of the VQIVYK hexapeptide and cysteine-containing R3 repeat region on the prion-like seeding potential of tau in tauopathies.

Cell treatment with buffer alone (containing transfection reagents), R2 and R3 fibrils or R1 and R4 samples did not affect cell number (Fig. 1H) or morphology (Fig. S3E). None of the peptides in monomeric forms affected seeding or cell number (data not shown).

3.3. Fibrils of minimal regions increase triton-insoluble phospho-tau levels and reseed intracellular tau

To examine tau phosphorylation changes, we collected biosensor cells 72 h after seeding with peptides assembled in the presence of heparin and fractionated them into Triton X-100-soluble and -insoluble fractions. Although there was no change in tau phosphorylation in total protein (Fig. S4A), the presence of Ser262-phosphorylated tau was evident in triton-insoluble fractions of cells treated with R2 and R3 fibrils (Fig. 2A). These results indicate that extracellular R2 and R3 fibrils increase the insolubility of intracellular tau following pathological phosphorylation that enhances the accumulation of seeded tau inclusions. However, this result did not answer whether the phosphorylation per se enhanced intracellular tau aggregation following seeding with extracellular R2 and R3 fibrils.

Biosensor cells express only the RD of tau (244–372 amino acids), and therefore, phosphorylation changes outside this domain cannot be examined. To overcome this limitation, we transiently expressed P301L Tau (0N4R) in HEK293 cells and then seeded them with peptide fibrils/samples for 72 h before cellular fractionation as described above. Similar to biosensor cells, there was no visible difference in tau phosphorylation in total protein (Fig. S4B). However, evident changes in total tau (Tau-5) and phosphorylated tau (Ser262, Ser396, Ser404) were noticeable in triton-insoluble fractions of cells treated with R2 and R3 fibrils (Fig. 2B). Additionally, both R2 and R3 fibrils resulted in tau oligomer (T22) formation in Tau P301L (0N4R) HEK293 cells. These findings suggest that only a small percentage of tau seeds derived from the minimum region are required to cause the formation of intracellular hyperphosphorylated tau aggregates.

Many reports suggest that the size and conformation of seeds impact the seeding activity of extracellular seeds [11,15,28]. Therefore, we next performed a reseeding assay to seed a new set of biosensor cells with total, triton-soluble, and -insoluble fractions of biosensor cells that had previously been seeded with peptide fibrils/samples. The reseeding assay revealed that all three fractions of R2 and R3 fibrils-treated cells resulted in intracellular Tau RD P301S aggregation (Fig. 3). This data indicates the fibrils of seeded tau acquired seeding potency similar to extracellular R2 and R3 fibrils.

4. Discussion

Tauopathies can be distinguished based on tau isoforms present in the filaments. While corticobasal degeneration, argyrophilic grain disease and progressive supranuclear palsy show 4R tau, Pick's disease (PiD) is characterised by the presence of only 3R isoform [29]. On the contrary, AD and chronic traumatic encephalopathy show the presence of both 3R and 4R tau isoforms [29]. Cryo-EM structural analysis of core filaments from brain tissues of tauopathy patients revealed that they all have a similar core area but diverse conformations [30]. The core structure is comprised of R3 and R4 along with 10–13 amino acids of the C-terminal domain, with different N-terminal extensions [30]. Structural and conformational differences between tau polymorphs in AD, PiD and other tauopathies, along with the effect of non-protein cofactors on tau aggregation, might affect the stability and propagation of aggregates [31]. Therefore, it is critical to identify tau regions that may play critical roles in differential tau aggregation and spread.

The hexapeptide amyloid motifs on R2 and R3 have been shown to assemble *in vitro* independently; however, they do not produce seed-competent fibrils [22]. Using peptides of individual repeats,

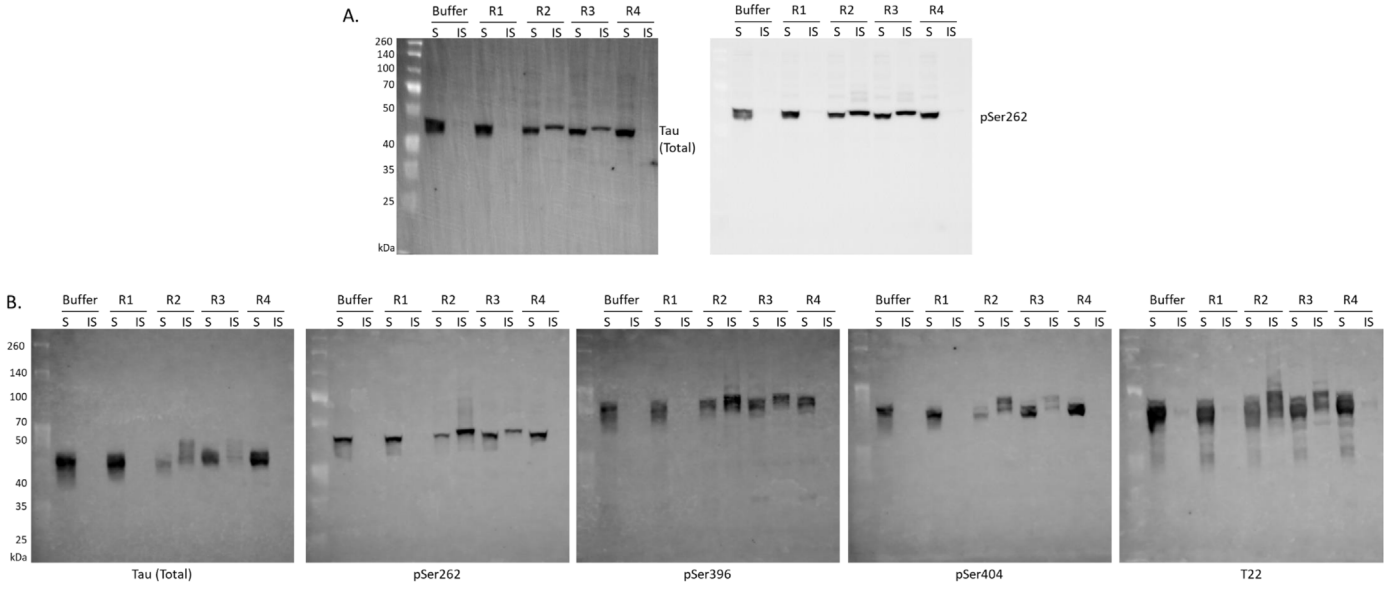

Fig. 2. Changes in intracellular tau phosphorylation. (A–B) Representative western blots of triton-soluble and -insoluble fractions after seeding Tau RD P301S biosensor cells (A) and Tau P301L (0N4R) HEK293 cells (B) with R1, R2, R3 and R4 samples/fibrils collected after 48 h of aggregation. n = 3. S, Triton-Soluble; IS, Triton-Insoluble. Buffer is the aggregation buffer containing heparin.

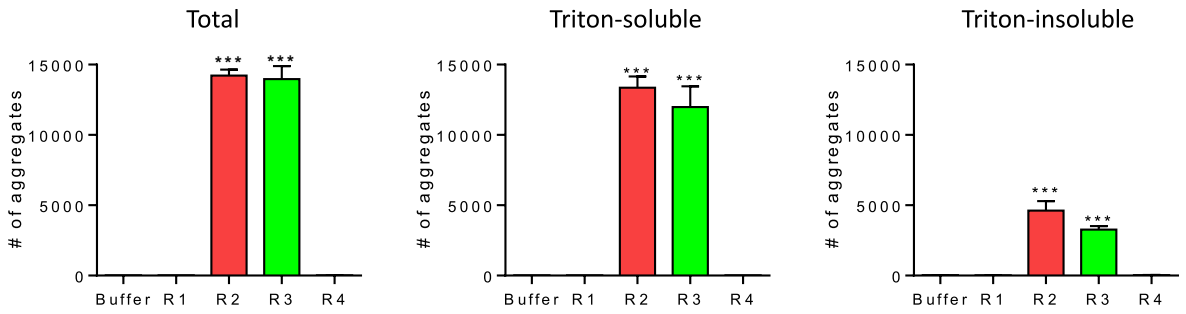

Fig. 3. Cellular reseeding assay. Quantification of intracellular Tau RD P301S aggregates in biosensor cells reseeded with the total, triton-soluble, and triton-insoluble fractions of cells seeded with buffer (containing heparin) or R1, R2, R3 and R4 samples or fibrils collected 48 h after heparin-supplemented *in vitro* aggregation assay. Data is mean ± SEM of 3 independent experiments. ***p < 0.001 *vs* buffer-treated cells, one-way ANOVA, Dunnett's posthoc test.

we show that R2, like R3, forms seed-competent fibrils, indicating that R2 may be a separate nucleus for tau aggregation. Although R2 aggregation was faster than R3, there was no difference in intracellular seeding by R2 and R3 fibrils. This suggests that the aggregation rate does not give differential potency to R2 and R3 seeds. Additionally, R3, but not R2, fibrils assembled without heparin were seed-competent, even though both R2 and R3 have identical N-terminal hexapeptide sequences and cysteine residues. These suggest that R3 may be the minimal region for pathological seed generation under physiological conditions, whereas R2 might need polyanionic cofactors to generate pathogenic seeds. The self-assembling R3 may nucleate tau aggregation in the absence of polyanionic cofactors, with R2 contributing in the later stages of the aggregation process. Additionally, R3 (C322A) formed fibrils when aggregated in the presence but not in the absence of heparin, explaining the role of heparin in remodelling the R3 or tau towards fibril-prone conformations, as highlighted in a recent *in silico* study [32]. Aggregates that are seed-competent may contain a mixture of monomers, oligomers, and fibrils. Since monomers do not seed intracellular tau aggregation, as demonstrated by us, further studies are required to identify and characterise the species type, oligomers or fibrils, in the aggregated sample responsible for the seeding effect.

Heparin-induced tau fibrils are polymorphic and different from fibrils derived from AD and PiD brains [33]. Several polyanionic cofactors such as RNA, lipids, and, recently DNA from several species of bacteria were found to promote tau aggregation *in vitro* [34–37]. The potential role of RNA in producing unique tau strains and their stability is also suggested in a recent preprint article by M Diamond's group [38]. Interaction of tau with cofactors enables the formation of metastable complexes that remain inert and reversible until the interaction with seeds, which triggers the formation of β-sheet containing species [39]. Despite studies demonstrating co-localisation of cofactors such as heparan sulfate and RNA with NFTs, Pick bodies, and neuritic plaques of AD and PiD, the role of polyanionic cofactors on tau pathological alterations has been overlooked [40,41].

A conserved motif in the middle of each RD of tau, KXGS, is required for tau binding to microtubules, local structural stabilisation, and oligomerisation [27]. *In vivo*, intermolecular disulfide bonds are formed when two cysteine residues in KXGS motifs, Cy291 in R2 and Cys322 in R3, oxidise, leading to tau dimerisation and fibrillisation. The two cysteine residues are functionally distinct and contribute differently to tau pathology [42]. Further, their positions differ in the fibrillar core, with R3 located in the fibril core and R2 in the fuzzy coat of fibrils [43]. Our data showing that R3 (C322A) fibrils formed in the presence of heparin are seed-competent suggests that C322 at the KXGS motif may play a role in tau seed generation under pathological conditions.

Tau propagation following seeding occurs either by template-dependent conformational changes or other unknown mechanisms [44]. Although PTMs are essential for a full-length tau to aggregate [45], it is unclear whether hyperphosphorylation is necessary for the seeded tau to aggregate. Our study aimed to investigate the hyperphosphorylation or solubility changes in endogenous seeded tau following cell seeding with fibrils of R2 and R3. Serine 262 phosphorylation appears early in AD pathogenesis [46], suggesting this phosphorylation may contribute to tau seed formation. Although we do not know which phosphorylations appeared first in our study, we can confirm that AD-specific phosphorylations in seeded tau appear in response to exogenous R2 and R3 fibrils. Our cell fractionation data show that cells seeded with R2 and R3 fibrils cause Ser262 phosphorylation in Tau RD P301S biosensor cells and other AD-specific phosphorylation, including Ser262, in Tau P301L (0N4R) HEK293 cells. In addition to phosphorylation, there is also oligomerisation of seeded P301L Tau. The presence of soluble phosphorylated tau in both the cell types suggests that mutation enhanced the phosphorylation (Fig. 2A and B), presumably making abnormally phosphorylated cytosolic tau prone to aggregate into insoluble inclusions upon exposure to seed-competent R2 and R3 fibrils. These findings suggest that pathological phosphorylation is one of the unknown factors contributing to the aggregation of intracellular seeded tau.

Our reseeding assay confirms that cell fractions (total or Triton-soluble and -insoluble) of cells previously seeded with R2 and R3 fibrils continue to display seeding activity. This data reconfirms that tau propagation is dependent not only on the initially generated fibrils but also on the newly formed tau inclusions. The intracellular tau inclusions with pathological phosphorylations presumably result from the failure of cell clearance mechanisms and phosphatase functions that define the ageing-associated molecular mechanisms involved in AD and other tauopathies. Altogether, evidence from our previous study [25], this study and other studies [26,42,43,47] support the importance of targeting the N-terminal hexapeptides or cysteines in R2 or R3 when developing tau aggregation and hyperphosphorylation inhibitors [48] or antibodies (Reviewed in Ref. [49]) for tau-targeted therapies. Since tau adopts disease-specific fibril polymorphs [15], a single inhibitor may not be capable of blocking seeding by all disease-associated polymorphs, possibly because both hexapeptide sequences contribute to differential seeding under different conditions.

5. Conclusion

Herein, we show that the two minimal tau regions, R2 and R3, are sufficient to seed intracellular tau aggregation, possibly via altering the composition of soluble hyperphosphorylated tau. R2 and R3 fibrils formed in the presence of heparin are seed-

competent. However, only R3 self-aggregates into seed-competent fibrils in the absence of heparin. Substitution of cysteine to alanine (C322A) in R3 affects its self-aggregation, inhibiting its seeding activity. Intriguingly, despite the substitution, R3 (C322A) assembles into seed-competent fibrils in the presence of heparin. These findings underline the importance of N-terminal hexapeptides and cysteine residues of R2 and R3 on tau aggregation, seeding and propagation. Our brief study sheds light on potential molecular mechanisms of seeded tau aggregation by tau repeat peptides of the microtubule-binding domain.

Authors' contribution

NA, LM and JM performed the experiments; NA, MH and VD critically analysed the data; NA and VD conceived the project and wrote the paper; All authors reviewed the results and approved the manuscript.

Data statement

All data presented are available upon reasonable request from Viswanath Das (viswanath.das@upol.cz).

Declaration of competing interest

The authors declare no conflict of interest related to this work.

Acknowledgements

The work was supported by the European Regional Development Fund (ENOCH, CZ.02.1.01/0.0/0.0/16_019/0000868), the Technology Agency of the Czech Republic (PerMed, TN01000013) and the Ministry of Education, Youth and Sports of the Czech Republic (EATRIS-CZ, LM2018133; Large RI Project LM2018129 - Czech-BioImaging), and Internal Student Grant Agency of the Palacky University in Olomouc, Czech Republic (IGA_LF_2021_038).

Appendix A. Supplementary data

Supplementary data to this article can be found online at https://doi.org/10.1016/j.biochi.2022.05.013.

References

[1] W. Noble, D. Hanger, C. Miller, S. Lovestone, The importance of tau phosphorylation for neurodegenerative diseases, Front. Neurol. 4 (2013) 83, https://doi.org/10.3389/fneur.2013.00083.
[2] H. Hampel, K. Blennow, L.M. Shaw, Y.C. Hoessler, H. Zetterberg, J.Q. Trojanowski, Total and phosphorylated tau protein as biological markers of Alzheimer's disease, Spec. Issue Biomark. Alzheimers Dis. Dement. Cerebrospinal Fluid Blood. 45 (2010) 30–40, https://doi.org/10.1016/j.exger.2009.10.010.
[3] K. SantaCruz, J. Lewis, T. Spires, J. Paulson, L. Kotilinek, M. Ingelsson, A. Guimaraes, M. DeTure, M. Ramsden, E. McGowan, C. Forster, M. Yue, J. Orne, C. Janus, A. Mariash, M. Kuskowski, B. Hyman, M. Hutton, K.H. Ashe, Tau suppression in a neurodegenerative mouse model improves memory function, Science 309 (2005) 476, https://doi.org/10.1126/science.1113694.
[4] A.B. Rocher, J.L. Crimins, J.M. Amatrudo, M.S. Kinson, M.A. Todd-Brown, J. Lewis, J.I. Luebke, Structural and functional changes in tau mutant mice neurons are not linked to the presence of NFTs, Beta-Amyloid Tau Protein Abnorm, Alzheimers Dis. 223 (2010) 385–393, https://doi.org/10.1016/j.expneurol.2009.07.029.
[5] Z. Berger, H. Roder, A. Hanna, A. Carlson, V. Rangachari, M. Yue, Z. Wszolek, K. Ashe, J. Knight, D. Dickson, C. Andorfer, T.L. Rosenberry, J. Lewis, M. Hutton, C. Janus, Accumulation of pathological tau species and memory loss in a conditional model of tauopathy, J. Neurosci. 27 (2007) 3650, https://doi.org/10.1523/JNEUROSCI.0587-07.2007.
[6] J. Miao, R. Shi, L. Li, F. Chen, Y. Zhou, Y.C. Tung, W. Hu, C.-X. Gong, K. Iqbal, F. Liu, Pathological tau from alzheimer's brain induces site-specific hyperphosphorylation and SDS- and reducing agent-resistant aggregation of tau in vivo, Front. Aging Neurosci. 11 (2019) 34, https://doi.org/10.3389/fnagi.2019.00034.
[7] W. Hu, X. Zhang, Y.C. Tung, S. Xie, F. Liu, K. Iqbal, Hyperphosphorylation determines both the spread and the morphology of tau pathology, Alzheimers Dement 12 (2016) 1066–1077, https://doi.org/10.1016/j.jalz.2016.01.014.
[8] F. Clavaguera, T. Bolmont, R.A. Crowther, D. Abramowski, S. Frank, A. Probst, G. Fraser, A.K. Stalder, M. Beibel, M. Staufenbiel, M. Jucker, M. Goedert, M. Tolnay, Transmission and spreading of tauopathy in transgenic mouse brain, Nat. Cell Biol. 11 (2009) 909–913, https://doi.org/10.1038/ncb1901.
[9] B. Frost, R.L. Jacks, M.I. Diamond, Propagation of tau misfolding from the outside to the inside of a cell, J. Biol. Chem. 284 (2009) 12845–12852, https://doi.org/10.1074/jbc.M808759200.
[10] A. Tarutani, H. Miyata, T. Nonaka, K. Hasegawa, M. Yoshida, Y. Saito, S. Murayama, A.C. Robinson, D.M.A. Mann, T. Tomita, M. Hasegawa, Human tauopathy-derived tau strains determine the substrates recruited for templated amplification, Brain 144 (2021) 2333–2348, https://doi.org/10.1093/brain/awab091.
[11] B. Falcon, A. Cavallini, R. Angers, S. Glover, T.K. Murray, L. Barnham, S. Jackson, M.J. O'Neill, A.M. Isaacs, M.L. Hutton, P.G. Szekeres, M. Goedert, S. Bose, Conformation determines the seeding potencies of native and recombinant tau aggregates, J. Biol. Chem. 290 (2015) 1049–1065, https://doi.org/10.1074/jbc.M114.589309.
[12] S. Boluda, M. Iba, B. Zhang, K.M. Raible, V.M.-Y. Lee, J.Q. Trojanowski, Differential induction and spread of tau pathology in young PS19 tau transgenic mice following intracerebral injections of pathological tau from Alzheimer's disease or corticobasal degeneration brains, Acta Neuropathol. 129 (2015) 221–237, https://doi.org/10.1007/s00401-014-1373-0.
[13] F. Clavaguera, H. Akatsu, G. Fraser, R.A. Crowther, S. Frank, J. Hench, A. Probst, D.T. Winkler, J. Reichwald, M. Staufenbiel, B. Ghetti, M. Goedert, M. Tolnay, Brain homogenates from human tauopathies induce tau inclusions in mouse brain, Proc. Natl. Acad. Sci. Unit. States Am. 110 (2013) 9535, https://doi.org/10.1073/pnas.1301175110.
[14] S.K. Kaufman, D.W. Sanders, T.L. Thomas, A.J. Ruchinskas, J. Vaquer-Alicea, A.M. Sharma, T.M. Miller, M.I. Diamond, Tau prion strains dictate patterns of cell pathology, progression rate, and regional vulnerability in vivo, Neuron 92 (2016) 796–812, https://doi.org/10.1016/j.neuron.2016.09.055.
[15] D.W. Sanders, S.K. Kaufman, S.L. DeVos, A.M. Sharma, H. Mirbaha, A. Li, S.J. Barker, A.C. Foley, J.R. Thorpe, L.C. Serpell, T.M. Miller, L.T. Grinberg, W.W. Seeley, M.I. Diamond, Distinct tau prion strains propagate in cells and mice and define different tauopathies, Neuron 82 (2014) 1271–1288, https://doi.org/10.1016/j.neuron.2014.04.047.
[16] S.K. Kaufman, T.L. Thomas, K. Del Tredici, H. Braak, M.I. Diamond, Characterisation of tau prion seeding activity and strains from formaldehyde-fixed tissue, Acta Neuropathol. Commun. 5 (2017) 41, https://doi.org/10.1186/s40478-017-0442-8.
[17] S.L. DeVos, B.T. Corjuc, D.H. Oakley, C.K. Nobuhara, R.N. Bannon, A. Chase, C. Commins, J.A. Gonzalez, P.M. Dooley, M.P. Frosch, B.T. Hyman, Synaptic tau seeding precedes tau pathology in human alzheimer's disease brain, Front. Neurosci. 12 (2018) 267, https://doi.org/10.3389/fnins.2018.00267.
[18] J. Vaquer-Alicea, M.I. Diamond, Propagation of protein aggregation in neurodegenerative diseases, Annu. Rev. Biochem. 88 (2019) 785–810, https://doi.org/10.1146/annurev-biochem-061516-045049.
[19] M.D. Mukrasch, J. Biernat, M. von Bergen, C. Griesinger, E. Mandelkow, M. Zweckstetter, Sites of tau important for aggregation populate β-structure and bind to microtubules and polyanions, J. Biol. Chem. 280 (2005) 24978–24986, https://doi.org/10.1074/jbc.M501565200.
[20] K. Tomoo, T.-M. Yao, K. Minoura, S. Hiraoka, M. Sumida, T. Taniguchi, T. Ishida, Possible role of each repeat structure of the microtubule-binding domain of the tau protein in in vitro aggregation, J. Biochem. (Tokyo) 138 (2005) 413–423, https://doi.org/10.1093/jb/mvi142.
[21] C. Despres, C. Byrne, H. Qi, F.-X. Cantrelle, I. Huvent, B. Chambraud, E.-E. Baulieu, Y. Jacquot, I. Landrieu, G. Lippens, C. Smet-Nocca, Identification of the Tau phosphorylation pattern that drives its aggregation, Proc. Natl. Acad. Sci. Unit. States Am. 114 (2017) 9080, https://doi.org/10.1073/pnas.1708448114.
[22] P. Ganguly, T.D. Do, L. Larini, N.E. LaPointe, A.J. Sercel, M.F. Shade, S.C. Feinstein, M.T. Bowers, J.-E. Shea, Tau assembly: the dominant role of PHF6 (VQIVYK) in microtubule binding region repeat R3, J. Phys. Chem. B 119 (2015) 4582–4593, https://doi.org/10.1021/acs.jpcb.5b00175.
[23] J. Stöhr, H. Wu, M. Nick, Y. Wu, M. Bhate, C. Condello, N. Johnson, J. Rodgers, T. Lemmin, S. Acharya, J. Becker, K. Robinson, M.J.S. Kelly, F. Gai, G. Stubbs, S.B. Prusiner, W.F. DeGrado, A 31-residue Peptide Induces Aggregation of Tau's Microtubule-Binding Region in Cells, Nat Chem. advance online publication, 2017, https://doi.org/10.1038/nchem.2754.
[24] J. Adamcik, A. Sánchez-Ferrer, N. Ait-Bouziad, N.P. Reynolds, H.A. Lashuel, R. Mezzenga, Microtubule-binding R3 fragment from tau self-assembles into giant multistranded amyloid ribbons, Angew. Chem. Int. Ed. 55 (2016) 618–622, https://doi.org/10.1002/anie.201508968.
[25] N. Annadurai, L. Malina, M. Salmona, L. Diomede, A. Bastone, A. Cagnotto, M. Romeo, M. Šrejber, K. Berka, M. Otyepka, M. Hajdúch, V. Das, Antitumour drugs targeting tau R3 VQIVYK and Cys322 prevent seeding of endogenous tau aggregates by exogenous seeds, FEBS J. (2021), https://doi.org/10.1111/febs.16270 n/a.
[26] P.M. Seidler, D.R. Boyer, J.A. Rodriguez, M.R. Sawaya, D. Cascio, K. Murray, T. Gonen, D.S. Eisenberg, Structure-based inhibitors of tau aggregation, Nat. Chem. 10 (2018) 170–176, https://doi.org/10.1038/nchem.2889.

[27] S. Ambadipudi, J.G. Reddy, J. Biernat, E. Mandelkow, M. Zweckstetter, Residue-specific identification of phase separation hot spots of Alzheimer's-related protein tau, Chem. Sci. 10 (2019) 6503–6507, https://doi.org/10.1039/C9SC00531E.

[28] Y. Tanaka, K. Yamada, K. Satake, I. Nishida, M. Heuberger, T. Kuwahara, T. Iwatsubo, Seeding activity-based detection uncovers the different release mechanisms of seed-competent tau versus inert tau via lysosomal exocytosis, Front. Neurosci. 13 (2019) 1258, https://doi.org/10.3389/fnins.2019.01258.

[29] Y. Shi, W. Zhang, Y. Yang, A.G. Murzin, B. Falcon, A. Kotecha, M. van Beers, A. Tarutani, F. Kametani, H.J. Garringer, R. Vidal, G.I. Hallinan, T. Lashley, Y. Saito, S. Murayama, M. Yoshida, H. Tanaka, A. Kakita, T. Ikeuchi, A.C. Robinson, D.M.A. Mann, G.G. Kovacs, T. Revesz, B. Ghetti, M. Hasegawa, M. Goedert, S.H.W. Scheres, Structure-based classification of tauopathies, Nature 598 (2021) 359–363, https://doi.org/10.1038/s41586-021-03911-7.

[30] J. Vaquer-Alicea, M.I. Diamond, L.A. Joachimiak, Tau strains shape disease, Acta Neuropathol. 142 (2021) 57–71, https://doi.org/10.1007/s00401-021-02301-7.

[31] Kim Chae, Haldiman Tracy, Kang Sang-Gyun, Hromadkova Lenka, Han Zhuang Zhuang, Chen Wei, Lissemore Frances, Lerner Alan, de Silva Rohan, Cohen Mark L., Westaway David, Safar Jiri G., Distinct populations of highly potent TAU seed conformers in rapidly progressing Alzheimer's disease, Sci. Transl. Med. 14 (n.d.) eabg0253. https://doi.org/10.1126/scitranslmed.abg0253.

[32] X. Dong, R. Qi, Q. Qiao, X. Li, F. Li, J. Wan, Q. Zhang, G. Wei, Heparin remodels the microtubule-binding repeat R3 of Tau protein towards fibril-prone conformations, Phys. Chem. Chem. Phys. 23 (2021) 20406–20418, https://doi.org/10.1039/D1CP02651H.

[33] W. Zhang, B. Falcon, A.G. Murzin, J. Fan, R.A. Crowther, M. Goedert, S.H. Scheres, Heparin-induced tau filaments are polymorphic and differ from those in Alzheimer's and Pick's diseases, Elife 8 (2019), e43584, https://doi.org/10.7554/eLife.43584.

[34] G. Tetz, M. Pinho, S. Pritzkow, N. Mendez, C. Soto, V. Tetz, Bacterial DNA promotes Tau aggregation, Sci. Rep. 10 (2020) 2369, https://doi.org/10.1038/s41598-020-59364-x.

[35] Y. Fichou, Y. Lin, J.N. Rauch, M. Vigers, Z. Zeng, M. Srivastava, T.J. Keller, J.H. Freed, K.S. Kosik, S. Han, Cofactors are essential constituents of stable and seeding-active tau fibrils, Proc. Natl. Acad. Sci. Unit. States Am. 115 (2018) 13234, https://doi.org/10.1073/pnas.1810058115.

[36] P.D. Dinkel, M.R. Holden, N. Matin, M. Margittai, RNA binds to tau fibrils and sustains template-assisted growth, Biochemistry 54 (2015) 4731–4740, https://doi.org/10.1021/acs.biochem.5b00453.

[37] C.G. Barracchia, R. Tira, F. Parolini, F. Munari, L. Bubacco, G.A. Spyroulias, M. D'Onofrio, M. Assfalg, Unsaturated fatty acid-induced conformational transitions and aggregation i.

[38] A.N. Zwierzchowski-Zarate, O.M. Kashmer, J.E. Collazo-Lopez, C.L. White, M.I. Diamond, RNA induces unique tau strains and stabilises Alzheimer's disease seeds, bioRxiv (2022), https://doi.org/10.1101/2022.01.29.478315, 2022.01.29.478315.

[39] Y. Fichou, Z.R. Oberholtzer, H. Ngo, C.-Y. Cheng, T.J. Keller, N.A. Eschmann, S. Han, Tau-cofactor complexes as building blocks of tau fibrils, Front. Neurosci. 13 (2019). https://www.frontiersin.org/article/10.3389/fnins.2019.01339.

[40] J.H. Su, B.J. Cummings, C.W. Cotman, Localisation of heparan sulfate glycosaminoglycan and proteoglycan core protein in aged brain and Alzheimer's disease, Neuroscience 51 (1992) 801–813, https://doi.org/10.1016/0306-4522(92)90521-3.

[41] S.D. Ginsberg, P.B. Crino, V.M.-Y. Lee, J.H. Eberwine, J.Q. Trojanowski, Sequestration of RNA in Alzheimer's disease neurofibrillary tangles and senile plaques, Ann. Neurol. 41 (1997) 200–209, https://doi.org/10.1002/ana.410410211.

[42] Y. Soeda, M. Yoshikawa, O.F.X. Almeida, A. Sumioka, S. Maeda, H. Osada, Y. Kondoh, A. Saito, T. Miyasaka, T. Kimura, M. Suzuki, H. Koyama, Y. Yoshiike, H. Sugimoto, Y. Ihara, A. Takashima, Toxic tau oligomer formation blocked by capping of cysteine residues with 1,2-dihydroxybenzene groups, Nat. Commun. 6 (2015) 10216, https://doi.org/10.1038/ncomms10216.

[43] A. Paul, G.K. Viswanathan, A. Huber, E. Arad, H. Engel, R. Jelinek, E. Gazit, D. Segal, Inhibition of tau amyloid formation and disruption of its preformed fibrils by Naphthoquinone–Dopamine hybrid, FEBS J. 288 (2021) 4267–4290, https://doi.org/10.1111/febs.15741.

[44] N. Kfoury, B.B. Holmes, H. Jiang, D.M. Holtzman, M.I. Diamond, Trans-cellular propagation of tau aggregation by fibrillar species, J. Biol. Chem. 287 (2012) 19440–19451, https://doi.org/10.1074/jbc.M112.346072.

[45] M.A. Meraz-Ríos, K.I. Lira-De León, V. Campos-Peña, M.A. De Anda-Hernández, R. Mena-López, Tau oligomers and aggregation in Alzheimer's disease, J. Neurochem. 112 (2010) 1353–1367, https://doi.org/10.1111/j.1471-4159.2009.06511.x.

[46] H. Lund, E. Gustafsson, A. Svensson, M. Nilsson, M. Berg, D. Sunnemark, G. von Euler, MARK4 and MARK3 associate with early tau phosphorylation in Alzheimer's disease granulovacuolar degeneration bodies, Acta Neuropathol. Commun. 2 (2014) 22, https://doi.org/10.1186/2051-5960-2-22.

[47] I. Aillaud, S. Kaniyappan, R.R. Chandupatla, L.M. Ramirez, S. Alkhashrom, J. Eichler, A.H.C. Horn, M. Zweckstetter, E. Mandelkow, H. Sticht, S.A. Funke, A novel D-amino acid peptide with therapeutic potential (ISAD1) inhibits aggregation of neurotoxic disease-relevant mutant Tau and prevents Tau toxicity in vitro, Alzheimer's Res. Ther. 14 (2022) 15, https://doi.org/10.1186/s13195-022-00959-z.

[48] M. Liu, T. Dexheimer, D. Sui, S. Hovde, X. Deng, R. Kwok, D.A. Bochar, M.-H. Kuo, Hyperphosphorylated tau aggregation and cytotoxicity modulators screen identified prescription drugs linked to Alzheimer's disease and cognitive functions, Sci. Rep. 10 (2020) 16551, https://doi.org/10.1038/s41598-020-73680-2.

[49] Y. Xia, S. Prokop, B.I. Giasson, Don't Phos over Tau": recent developments in clinical biomarkers and therapies targeting tau phosphorylation in Alzheimer's disease and other tauopathies, Mol. Neurodegener. 16 (2021) 37, https://doi.org/10.1186/s13024-021-00460-5.